

Supplementary Information

Revealing the Catalytic Kinetics and Dynamics of Individual Pt Atoms at Single-Molecule Level

Xiaodong Liu^{a,b,c,†}, Xin Ge^{d,†}, Jing Cao^{a,b,†}, Yi Xiao^{a,b}, Yan Wang^d, Wei Zhang^{d,*}, Ping Song^{a,b,*},
Weilin Xu^{a,b*}

^aState Key Laboratory of Electroanalytical Chemistry, & Jilin Province Key Laboratory of Low Carbon Chemical Power, Changchun Institute of Applied Chemistry, Chinese Academy of Sciences, 5625 Renmin Street, Changchun 130022, P.R. China.

^bUniversity of Science and Technology of China, Anhui 230026, China.

^cWenzhou Institute, University of Chinese Academy of Sciences, Wenzhou 352001, China

^dKey Laboratory of Mobile Materials MOE, and School of Materials Science & Engineering, and Electron Microscopy Center, and International Center of Future Science, Jilin University, Changchun 130012, China

[†]These authors contribute equally to this work.

*To whom correspondence, Ping Song, Wei Zhang, Weilin Xu

Email: songping@ciac.ac.cn (P. S.), weizhang@jlu.edu.cn (W. Z.), weilinxu@ciac.ac.cn (W. X.)

Single-molecule reaction experiments

Single-molecule fluorescence measurements were performed on a homebuilt prism-type total internal reflection (TIR) fluorescence microscope based on an Olympus IX71 inverted microscope. A continuous wave circularly polarized 532 nm laser beam (CrystaLaser, GCL-025-L-0.5%) of 4-5mW was focused onto an area of $\sim 80 \times 80 \mu\text{m}^2$ on the sample to directly excite the fluorescence of product, which was collected by a 60X NA1.2 water-immersion objective (UPLSAPO60XW, Olympus). The fluorescence of resorufin was filtered by two filters (HQ550LP, HQ580m60), and projected onto a camera (AndoriXon EMCCD with EM Gain=120, DU-897U-CS0-#BV), which was controlled by an Andor IQ software. All optical filters are from Chroma Technology Corp. The movies are analyzed using a home-written IDL program (written and permitted by Peng Chen

group at Cornell University), which can extract the fluorescence intensity trajectories from localized fluorescence spots individually across the entire movie. The intensity of each bright spot in an image is obtained by integrating the signal counts over an area of $\sim 1 \times 1 \mu\text{m}^2$.

The measurement was carried out in a flow cell, 100 μm (height) \times 2 cm (length) \times 5 mm (width), formed by double-sided tapes (3M) sandwiched between a quartz slide (Technical Glass) and a borosilicate coverslip (Gold Seal). 100 μL of Pt-nanoparticles solution was dropped onto quartz slide, and kept for 40 min and then rinsed with amount of MilliQ water to remove unbound nanoparticles. The edges of the coverslip were sealed by 5 minute-epoxy (Devcon). Two holes were drilled on the quartz slide to connect to polyethylene tubing (Instech Laboratories, 0.76mm ID) and a syringe pump for continuous solution flow at 10 μL /minute.

Experimental methods

Materials and reagents

Platinum(IV) chloride (> 99.99%), Cerium(III) nitrate hexahydrate (>99.999%), Propionic acid (ACS reagent, $\geq 99.5\%$), Ethylene glycol (anhydrous, 99.8%) were purchased from Aladdin. These chemicals were used as received without further purification. Ultrapure Millipore water (18.2 M Ω cm) was used as the solvent throughout. Reactant Resazurin was purchased from Sigma-Aldrich. The hydrogen was produced by the hydrogen generator.

Synthesizing and characterization of nanoceria-supported atomically dispersed Platinum catalysts

For the preparation of Pt@CeO₂, it was dependent on the literature (1). The synthetic process was conducted by following these steps. Firstly, 1.0 g Ce(NO₃)₃·6H₂O and 6.90 mg PtCl₄ were dissolved in 1 mL deionized water. 1 mL of propionic acid and 30 mL of ethylene glycol were added to the above solution with stirring. Then the uniformly mixed solution was sealed in an autoclave and heated at 160 °C for 3 h. The product was collected by centrifugation (10000 rpm, 10 minutes) and washed thoroughly with DI water and dry ethanol. It was dried at 110 °C in air for 5 h. Then it was disposed at 300 °C for another 2 h to remove residual water or organics. The obtained product was calcined in air at 1000 °C for 2 h, which produced atomically dispersed Pt supporting on nanoceria. CeO₂ nanocrystals were synthesized in a similar way without adding the Pt salt.

The morphology and structure of Pt SAC and Pt nanoparticles were characterized using aberration-corrected high-angle annular dark-field scanning transmission electron microscopy (HAADF-STEM) and the high resolution TEM (HRTEM) obtained on a JEM ARM 300F GRAND ARM, transmission electron microscopy (TEM) with an accelerating voltage of 300kV. To monitor the catalysis-induced surface variation, marked TEM grids were adopted to localize precisely the position of individual particles before and after catalytic process.

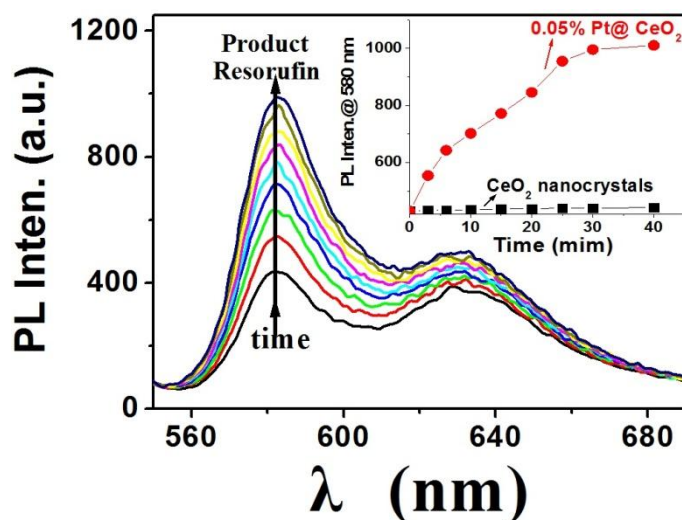


Fig. S1 The reduction reaction of nonfluorescent resazurin to highly fluorescent resorufin by H_2 catalyzed by $Pt_1@CeO_2$ (with Pt loading 0.05%).

The calculation of Pt loading of $Pt_1@CeO_2$ for single molecule experiment:

For the case here, the mass density of the obtained CeO_2 nanocrystals is about 1.9 g/cm^3 . With its average size of about 112 nm as shown in the following Scheme S1, the volume of a single crystal is about 1300000 nm^3 , then the mass of a single CeO_2 nanocrystal is about $2.4 \times 10^{-15}\text{ g}$, the mass of a single Pt atom is about $32.4 \times 10^{-23}\text{ g}$, then when there is only one Pt atom sitting on a single CeO_2 nanocrystal, the average Pt content on $Pt_1@CeO_2$ is about 0.000014 wt.% \sim 0.14 ppm. In this case, the real Pt loading of $Pt_1@CeO_2$ for single-molecule experiments is about 0.1 ppm, then about 30% of CeO_2 nanocrystals are bare without Pt.



Scheme S1 The loading of single Pt atom on single CeO_2 nanocrystal with size of about 112 nm for the calculation of Pt content.

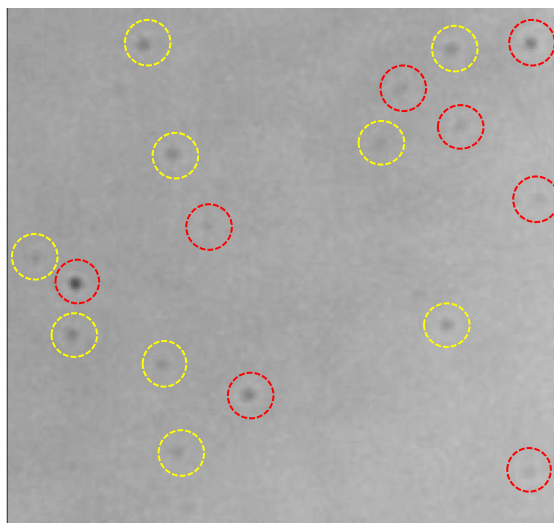


Fig. S2 The typical bright-field image to show the sparse distribution of individual CeO₂ nanocrystals in the flow cell. The yellow circles indicate that the fluorescence signal can be detected in the subsequent fluorescence detection model and confirm the existence of Pt atoms on their surfaces; the red circles indicate that no fluorescence signal can be detected and then no Pt on their surfaces.

By counting the numbers of these two different types of particles from multiple areas in different flow cells, statistically, we found that about 32% of these observed particles are inactive for the reaction, indicating no Pt on them.

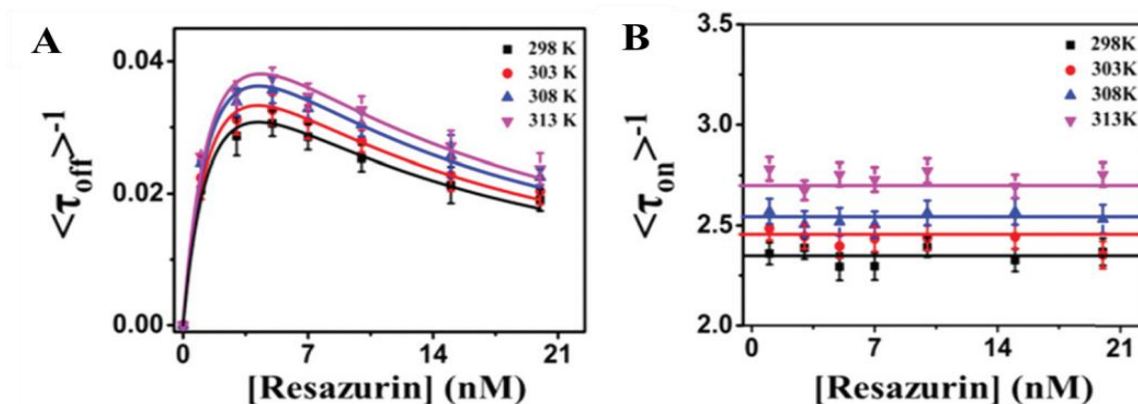


Fig. S3 (A) and (B) Single-molecule catalytic kinetics of Pt nanoparticles with size of about 4.9 nm at different temperatures. The product formation rates ($\langle \tau_{off}^{-1} \rangle$) (A) are dependent on the resazurin concentration and temperature, and the product dissociation rates ($\langle \tau_{on}^{-1} \rangle$) (B) are independent of the resazurin concentration but dependent on temperature. Each data point is averaged over above 90 turnover trajectories from the nanoparticles. This plot was cited from Ref(2) for a comparison with Pt SAC.

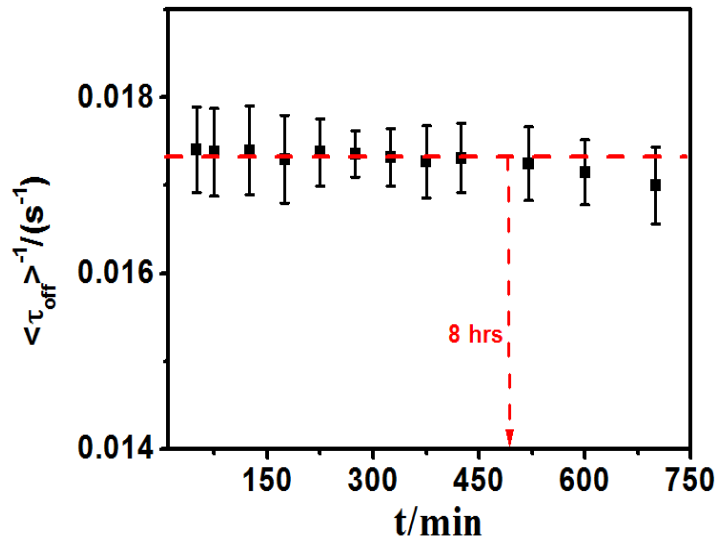


Fig. S4 The time-dependent catalytic activity (product formation rates, $\langle \tau_{\text{off}}^{-1} \rangle$) averaged from >70 trajectory at 18 nM resazurin with saturated H_2 .

Based on the fact shown in above Fig. S4, to avoid the effect from the possible deactivation, each data-point shown in Fig. 3 and Fig. 4 was obtained from fresh $\text{Pt}_1@ \text{CeO}_2$ by collecting the data within the first 2-3 hours after the starting of the catalytic process.

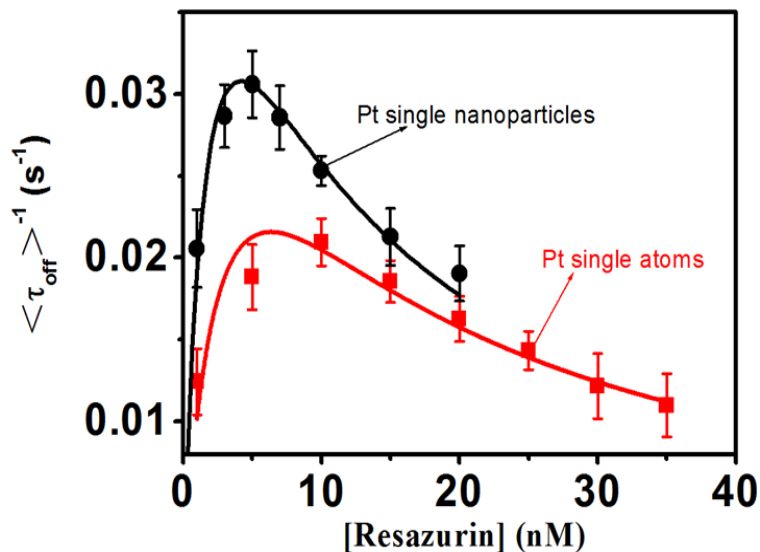


Fig. S5 Single-molecule catalytic kinetics of $\text{Pt}_1@ \text{CeO}_2$ (red curve) and Pt NPs (black curve) with size of about 4.9 nm at 298 K. The data about Pt NPs were cited from Ref(2) for a comparison with Pt SAC.

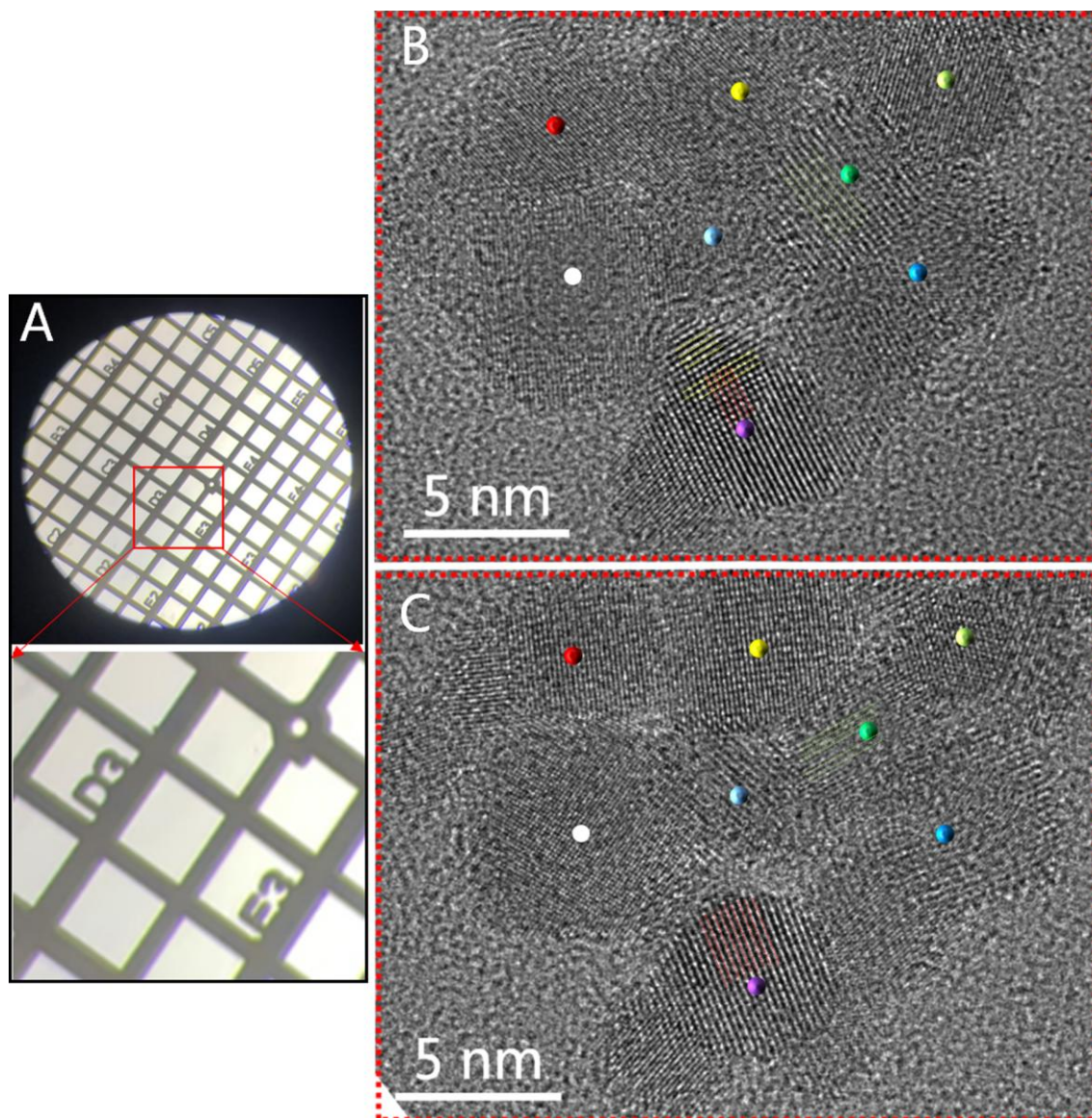


Fig. S6 (A) Commercial Cu grid marked with numbers and letters. HRTEM images of the same group Pt nanoparticles before (B) and after (C) a long-term (10 hrs) catalytic reduction reaction of resazurin by H_2 obtained based on the marked TEM grid shown in (A). The dots in 8 different colors shown in both (B) and (C) indicate the spatial distribution of 8 individual Pt nanoparticles before and after the catalytic process. Tremendous variation of surface structure can be seen clearly after catalytic process. Such tremendous variation of surface structure revealed here indicates that the active sites are very dense and crowded on surfaces of Pt NPs. The lines in different colors in (B) and (C) exemplify the surface variation on the same particles after catalysis.

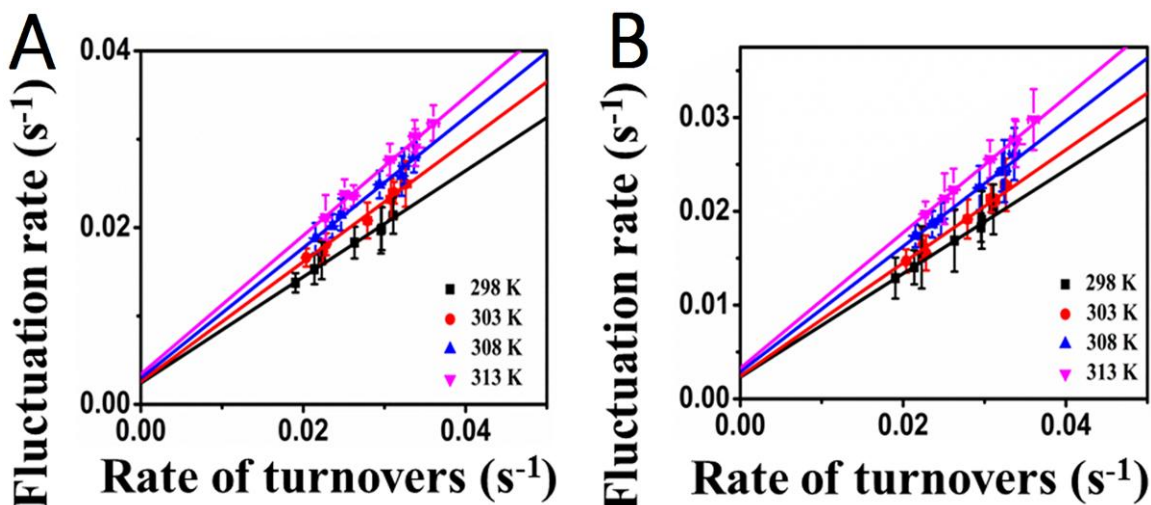


Fig. S7 (A and B) Dependence of the activity fluctuation rates on the turnover rates for the τ_{off} process (A) and τ_{on} process (B) at different temperatures. Solid lines are linear fits. This plot was cited from Ref(2) for a comparison with Pt SAC.

DFT Calculation for reactant and product molecules on the surface of Pt nanoparticle and Pt₁@CeO₂

All the electronic structure calculations have been carried out through density functional theory (DFT) method in the Vienna ab initio simulation package (VASP) (3-4) with the projector augmented-wave method to treat electron-ion interactions (5). The Perdew–Burke–Ernzerhof (PBE) form of the Generalized-Gradient Approximation (GGA) was employed to describe electron exchange and correlation (6). The wave functions at each k-point were expanded with a plane wave basis set and a kinetic cutoff energy up to 400 eV. Brillouin zone integration was approximated by a sum over special selected k-points using the Monkhorst–Pack method and they were set to 2×2×1. The electron occupancies were determined using Gaussian broadening with a width of 0.05 eV. Spin-polarized DFT+U (7-8) calculations with a value of $U_{\text{eff}}=6.0$ eV for Ce 4f state were applied to correct the strong electron-correlation properties of CeO₂ (9). The convergence criteria for the energy was set to 1.0×10^{-4} eV. The vacuum slab thickness was 15 Å to avoid interactions between different slabs. During the calculation process, Pt(111) surface was modeled by four-atomic-layer supercells with the bottom two layers fixed, and CeO₂(111) surface was modeled by nine-atomic-layer supercells with the bottom three layers fixed. According to the experimental result, the Pt substitutes Ce atom on the ceria surface and is surrounded by up to six nearby oxygen atoms. The adsorption energy can be used to describe the variation of total energy of each species before and after adsorption. In the current work, the adsorption energy (E_{ad}) was calculated based on the equation:

$$E_{\text{ad}} = E_{\text{substrate+adsorbate}} - (E_{\text{adsorbate}} + E_{\text{substrate}}) \quad (1)$$

And the binding energy (E_{b}) for Pt atom was calculated based on the equation:

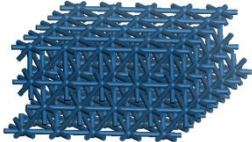
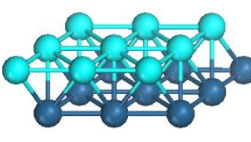
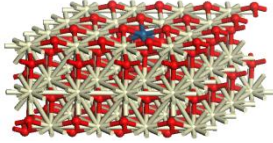
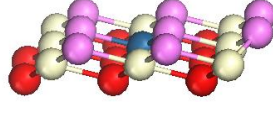
$$E_b = E_{\text{substrate+Pt1}} - (E_{\text{Pt1}} + E_{\text{substrate}}) \quad (2)$$

where $E_{\text{substrate+adsorbate}}$ is the total energy of the molecule adsorption system in the equilibrium state on different surfaces; $E_{\text{adsorbate}}$ and $E_{\text{substrate}}$ are the total energies of the free adsorbed molecule and residual surfaces, respectively. $E_{\text{substrate+Pt1}}$ is the total energy for different surfaces; E_{Pt1} and $E_{\text{substrate}}$ are the energy for Pt atom and the surface excepted for Pt atom. With this definition, a negative value corresponds to the stable adsorption on corresponding surfaces. Moreover, the surface energy E_{surf} for two surfaces was considered. Herein, E_{surf} for Pt(111) was calculated on the equation as followed:

$$E_{\text{surf}} = (E_{\text{total}} - N * E_{\text{bulk}}) / 2A \quad (3)$$

Where E_{total} was the total energy for the system, E_{bulk} was the energy of single atom in bulk structure, N was the atom numbers in the supercell, and A was the cross section area for slab. For $\text{Pt}_1@ \text{CeO}_2$ surface, the chemical potentials for redundant atoms excepted for stoichiometric ratio should be considered in E_{bulk} . The calculated surface for Pt(111) was 0.190 eV and 0.090 eV for $\text{Pt}_1@ \text{CeO}_2$.

Table S1. The supercell structures for Pt_n and $\text{Pt}_1@ \text{CeO}_2$ with enlarged partial view.

System	^a Structure	^b Partial	E_{surf}
Pt_n			0.090
$\text{Pt}_1@ \text{CeO}_2$			0.190
Note: The balls with red/pink, yellow and blue/light blue represented O, Ce and Pt atoms respectively, and the pink balls represented oxygen atoms on surface layer. ^a Structure and ^b Partial represented the complete structure for calculation and partial structure including Pt. Unit for E_{surf} : eV/Å ²			

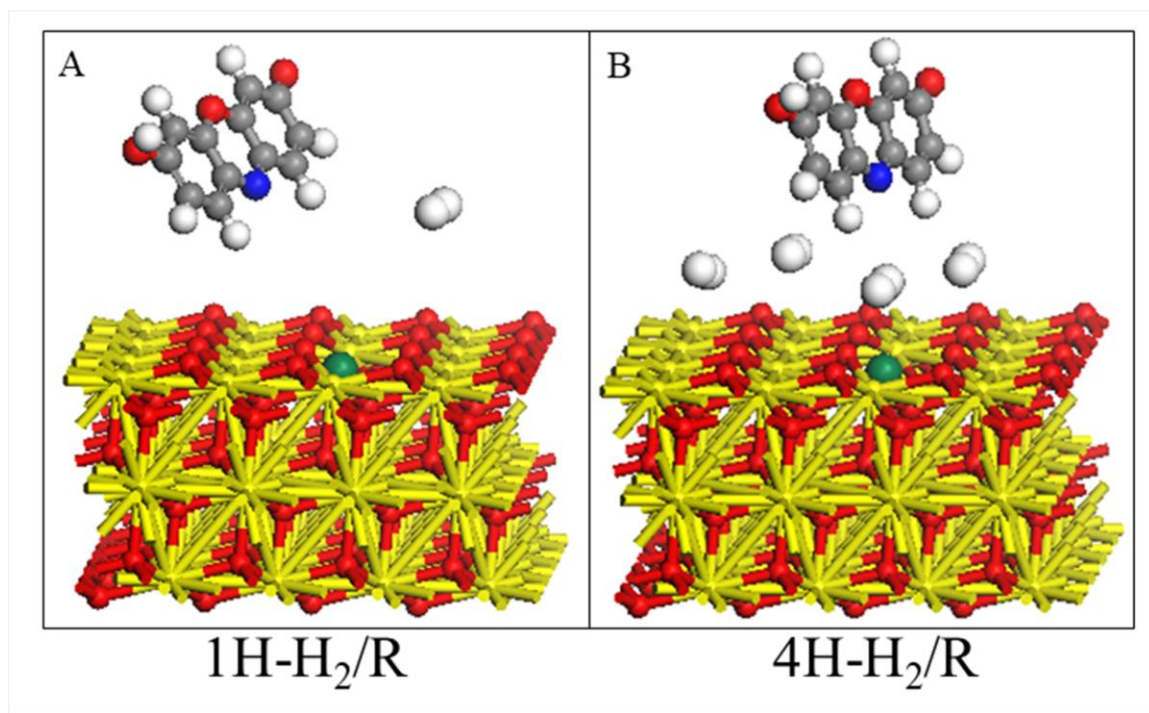


Fig. S8 The schematic diagram for considering one (A) and four (B) H₂ molecules with one resazurin molecule on Pt₁@CeO₂ surface, similar with that on Pt_n surface. The green balls represent individual Pt atoms.

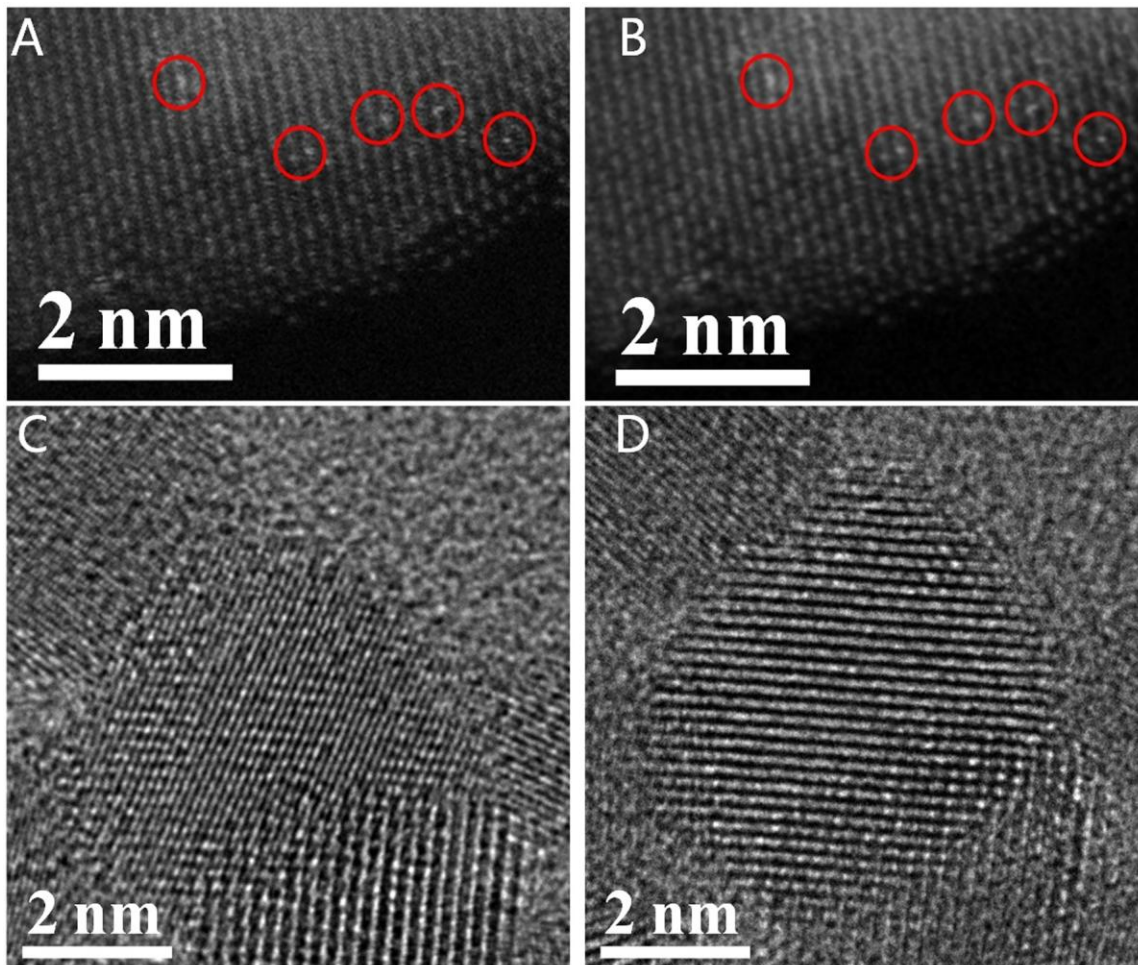


Fig. S9 (A, B) The HAADF-STEM images for the same location to show the stability of Pt atoms (marked with red circles) on support CeO₂ nanocrystal surface (with Pt loading of 0.05 wt%) before (A) and after (B) a long-term (10 hrs) catalytic reduction reaction of resazurin by H₂. (C, D) HRTEM analysis to show the surface variation of a Pt nanoparticle before (C) and after (D) a long-term (10 hrs) catalytic reduction reaction of resazurin by H₂.

Supplemental References

1. P. Xie, T. Pu, A. Nie, S. Hwang, S. Purdy, W. Yu, D. Su, J. Miller, C. Wang, Nanoceria- Supported Single-Atom Platinum Catalysts for Direct Methane Conversion. *ACS Catal.* **8**, 4044-4048 (2018).
2. X. Liu, T. Chen, W. Xu, Revealing the thermodynamics of individual catalytic steps based on temperature-dependent single-particle nanocatalysis. *Phys.Chem.Chem.Phys.* **21**,21806-21813(2019).

3. G. Kresse,; J. Furthmüller, Efficiency of ab-initio total energy calculations for metals and semiconductors using a plane-wave basis set. *Comput. Mater. Sci.* **6**, 15(1996).
4. G. Kresse, J. Furthmüller, Efficient iterative schemes for ab initio total-energy calculations using a plane-wave basis set. *Phys. Rev. B: Condens. Matter Mater. Phys.* **54**, 11169 (1996).
5. G. Kresse, D. Joubert, From ultrasoft pseudopotentials to the projector augmented-wave method. *Phys. Rev. B: Condens. Matter Mater. Phys.* **59**, 1758 (1999).
6. J. P. Perdew, K. Burke, M. Ernzerhof, Generalized gradient approximation made simple. *Phys. Rev. Lett.* **77**, 3865 (1996).
7. S. Dudarev, G. Botton, S. Savrasov, C. Humphreys, A. Sutton, Electron-energy-loss spectra and the structural stability of nickel oxide: An LSDA+U study. *Phys. Rev. B: Condens. Matter Mater. Phys.* **57**, 1505 (1998).
8. V. I. Anisimov, F. Aryasetiawan, A. Lichtenstein, Firstprinciples calculations of the electronic structure and spectra of strongly correlated systems: the LDA+U method. *J. Phys.: Condens. Matter* **9**, 767(1997).
9. C. Sevik, T. Çağın, Mechanical and electronic properties of CeO₂, ThO₂, and (Ce, Th) O₂ alloys, *Phys. Rev. B* **80**, 014108-1(2009).